Title

Dual Wet and Dry Resilient Cellulose II Fibrous Aerogel for Hydrocarbon–Water Separation and Energy Storage Applications

Journal

ACS Omega, 3(3)

ISSN

2470-1343

Authors

Jiang, Feng
Hsieh, You-Lo

Publication Date

2018-03-31

DOI

10.1021/acsomega.8b00144

Peer reviewed

ACS OMEGA

Article

Cite This: ACS Omega 2018, 3, 3530−3539

Dual Wet and Dry Resilient Cellulose II Fibrous Aerogel for Hydrocarbon−Water Separation and Energy Storage Applications

Feng Jiang† and You-Lo Hsieh*

Fiber and Polymer Science, University of California, Davis, California 95616, United States

Supporting Information

ABSTRACT: Cellulose fibrous aerogels have been fabricated by a facile and aqueous process that disintegrated electrospun cellulose fibers (ECFs) and reassembled via freezing/freeze-drying with significantly improved dry resiliency and spontaneous 89% shape recovery from ca. 70% compressive strain. Owing to the resilient and 200−300 nm wide ECFs, the cellulose fibrous aerogels exhibited excellent dual dry and wet resiliency as well as improved pore accessibility. The fibrous cellular walls interconnect the aerogel pore structure to allow extraordinary liquid absorption capacity up to 373 g/g, accounting for 95% of the theoretical absorption capacity. Both highly dry resilient and absorbent properties of the ECF aerogel are highly advantageous for hydrocarbon/oil contamination removal and for hydrocarbon/water separation applications. In addition, the ECF aerogel could be carbonized into carbon aerogel in supercapacitors for energy storage.

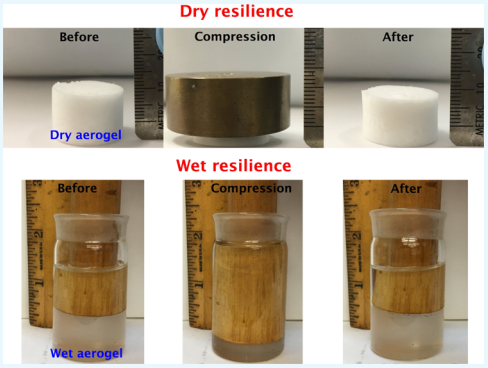

INTRODUCTION

Aerogels are ultralightweight porous materials often fabricated from inorganic,[1−3] synthetic polymeric,[4−6] and carbonaceous[7−9] precursors by complicated and costly processes. Because of their super low densites, that is, close to air, aerogels typically suffer from irreversible deformation or even brittleness when compressed. Aerogels have also been made from renewable regenerated cellulose and cellulose derivatives such as cellophane, viscose, and nitrocellulose as early as 1932.[10] Most cellulose aerogels reported to date are based on dissolution and regeneration of cellulose that require significant quantities of solvents and chemicals.[11−14] A much greener process in fabricating cellulose aerogel was more recently demonstrated by freezing and freeze-drying of sulfuric acid-hydrolyzed cellulose nanocrystals[15−17] and cellulose nanofibrils produced by enzymatic hydrolysis and mechanical defibrillation,[18] TEMPO oxidation,[19−22] carboxymethylation,[23,24] and mechanical (homogenization[25−27] or ultrasonication[28]) processes. Because the Young's modulus of cellulose I has been reported in the range of 138−155 GPa,[29−31] which is much higher than the 88−98 GPa[29,30] values for regenerated cellulose II, aerogels constructed from nanocellulose are expected to have better mechanical properties than those with a regenerated cellulose allomorph. Indeed, nanocellulose aerogels have shown outstanding cyclic wet compressive resilience with almost full shape recovery in water within seconds[15,25] and to withstand over 80% compression in the dry state while staying intact.[22,32−34] However, dry compression leads to irreversible deformation of nanocellulose aerogels whose dry resilience has only been improved by chemical modification with silane[35,36] or incorporation of reduced graphene oxide[37] and polypyrrole.[38] Dry resilient aerogels from nanocellulose alone have not been reported to date.

Most recently, aerogels have also been fabricated from synthetic fibers generated by electrospinning, a versatile way to produce fine submicron fibers from polymer solutions or melts,[39] including polyacrylonitrile with a tetraethyl orthoslicate silica precursor in camphene[40] or a water/*tert*-butanol mixture,[4] methylacrylate copolymer in dioxane,[41] polyacrylonitrile with graphene oxide in water,[42] and polycaprolactone in water,[43] then frozen and freeze-dried. These aerogels from electrospun fibers could recover almost completely from compression in the dry state, and such compression resiliency was attributed to their large fiber dimensions (a few hundred nm in width) in general and chemical cross-linking.[4,40]

Previously, we have developed a versatile and robust process to generate ultrafine cellulose fibers by electrospinning cellulose acetate followed by hydrolysis.[44] It is thus plausible to construct more dry resilient cellulose aerogels from these electrospun cellulose fibers (ECFs). ECFs are considered to be an excellent precursor to fabricate more dry resilient cellulose aerogels because of their typically larger diameters in the range of 200−300 nm and yet being hydrophilic and easily aqueous dispersible, making dispersion a green process. The abundant surface hydroxyl groups on cellulose fibers offer vast possibility for surface modification, leading to facilely tunable surface chemistry and properties.

Received: January 23, 2018
Accepted: March 12, 2018
Published: March 26, 2018

DOI: 10.1021/acsomega.8b00144
ACS Omega 2018, 3, 3530−3539

RESULTS AND DISCUSSION

The ECF membrane derived from cellulose acetate and hydrolyzed back to cellulose appeared white, ultrathin, and paper-like film, consisting of submicrometer-sized fibers with 262 ± 79 nm average width (Figure S1, Supporting Information). The ECF membrane was cut into 5 × 5 mm pieces and homogenized into an aqueous dispersion by high-speed blending (37 000 rpm, 5 min). The fibers in the dispersion remained similar in widths as original ECF but were significantly shortened to ca. 50−300 μm long and slightly entangled (Figure 1a,b). While the blending shear force reduced the fiber length by over 10 fold, the aspect ratios of the homogenized fibers remained high at up to ca. 1000.

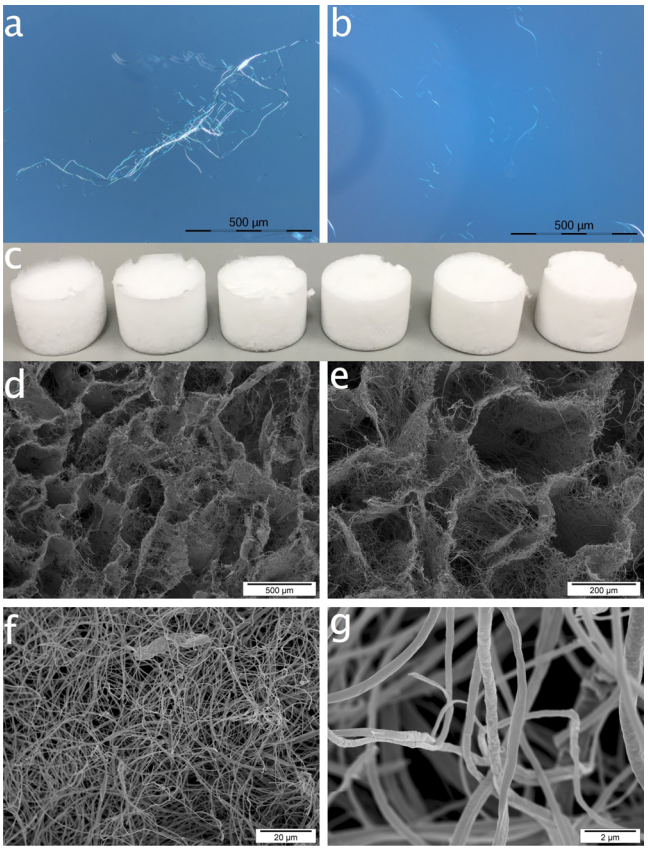

Figure 1. ECFs by optical microscopy under cross-polarizers: (a) before, (b) after high-speed blending homogenization; (c) ECF aerogels assembled from aqueous dispersions of ECFs at 0.1, 0.2, 0.3, 0.4, 0.5, and 0.6 wt % from left to right; (d−g) scanning electron microscopy (SEM) images of ECF aerogel assembled from 0.4 wt % aq ECF dispersion.

Freezing (−20 °C, 5 h) and then lyophilizing (−50 °C, 24 h) the homogenized aqueous ECF dispersions (0.1−0.6 wt %) produced white aerogels without appreciable dimensional change, indicating the absence of shrinkage from freezing and freeze-drying (Figure 1c). These aqueous dispersion and freezing/freeze-drying processes convert the planar fibrous web into hierarchical porous structures of large several hundred micrometer wide cellular networks (Figure 1d,e) with the surrounding fibrous walls containing several tens of micrometer wide interfiber spacings (Figure 1f,g). The large cellular pores are hexagonal, shaped by the slow nucleation of ice into large crystals, 1 order of magnitude larger than the interfiber spacings and 3 orders of magnitude larger than the ECFs. Similar hierarchical porous structures were observed on all aerogels, although the macropores appeared much larger and more irregularly shaped on those fabricated from lower ECF concentrations (Figure S2, Supporting Information). The 200−300 nm wide fibers in all aerogels are similar to those originally electrospun, again confirming no change in their lateral dimensions from blending and assembling. On the cellular pore walls of the ECF aerogel, the fibers overlay on one another, forming a loose network structure or highly porous walls. Our previous findings showed that by the same freezing and freeze-drying processes, the much narrower (1−2 nm) cellulose nanofibrils (CNFs) can assemble into film-like structures without distinction among the individual CNFs.[22] The lacking of interfiber association for ECF aerogel is partially attributed to the 2 orders magnitude larger and highly irregular fiber widths and shapes.

With increasing aq. ECF dispersion concentrations from 0.1 to 0.6 wt %, the ECF aerogel densities increased linearly from 1.1 to 7.0 mg/cm^3 and their corresponding porosities decreased linearly from 99.9 to 99.6% (Figure 2a). Aqueous alkaline hydrolysis converts the amorphous electrospun cellulose acetate (ECA) into regenerated cellulose structures with three crystalline peaks at 2θ of 12.1°, 19.8°, and 21.8° (Figure 2b), corresponding to the 1−10, 110, and 020 lattice planes of cellulose II,[47,48] respectively. The assembled ECF aerogel had a similar X-ray diffraction (XRD) spectrum as the precursor ECF membrane, showing the same cellulose structure. The crystallinity index (CrI) was 71.6 and 69.3% for ECF membrane and aerogel, respectively. The slightly lowered crystallinity of the aerogel could be ascribed to mechanical agitation. The Brunauer−Emmett−Teller (BET) nitrogen adsorption isotherm showed nearly reversible adsorption and desorption loops without leveling off at a high relative pressure (Figure 2c), which is typical of type II adsorption isotherms of nonporous and macroporous structures. The pore size distribution curve showed a broad distribution of meso- and macropores ranging from 20 to 90 nm (Figure 2d), further corroborating the smaller interfiber pores on the cellular walls surrounding the macroscopic cellular pores previously observed by SEM. The specific surface and pore volume of cellulose fiber aerogel are 7.9 m^2/g and 0.016 cm^3/g, respectively, which are close to the respective 7.6 m^2/g and 0.015 cm^3/g values of the original electrospun cellulose membrane (Figure S3, Supporting Information), as expected. It should be noted that the pore volume determined by the BET measurement involves the micro-/mesopores and has little effect on the liquid absorption capacity discussed below. The fibers in the aerogels are essentially isolated from each other, similar to the electrospun membrane, but bimodally distributed spatially in the more highly concentrated fibrous walls and much more separated from each other by large hundreds of micrometer size spaces generated by large ice crystals from slow freezing. As noted earlier, the regenerated cellulose ECFs do not exhibit the ability to self-assemble into the contact film as CNFs, a distinction attributed to the Cellulose II structure of ECFs as opposed to the CNF Cellulose I structure as well as the 2 orders of magnitude lower specific surface for interfiber association of the much wider ECF than CNFs, that is, ca. 200 nm versus 2 nm, respectively.

The ECF aerogels remained intact and were highly stable in organic liquids, showing very high absorption capacities toward organic liquids, as demonstrated by the 201−373 g/g of

DOI: 10.1021/acsomega.8b00144
ACS Omega 2018, 3, 3530−3539

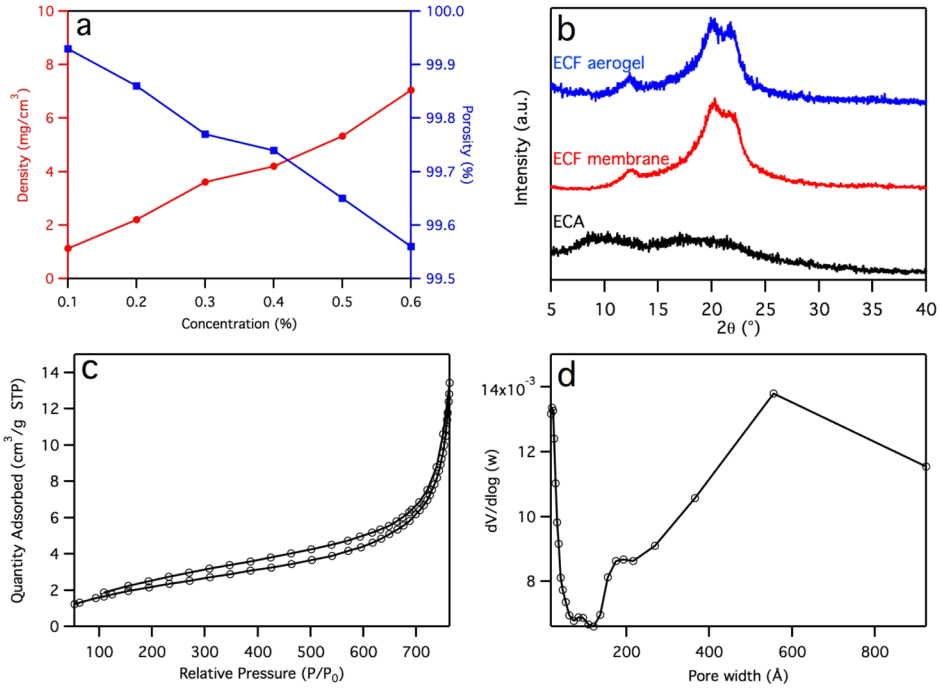

Figure 2. ECF aerogel structures: (a) density and porosity vs aq dispersion concentration; (b) XRD spectra of ECA, hydrolyzed ECF membrane and aerogel; (c) N_2 adsorption−desorption isotherm; and (d) pore size distribution. The ECF aerogel used in XRD and BET measurement was assembled from the 0.5 wt % concentration.

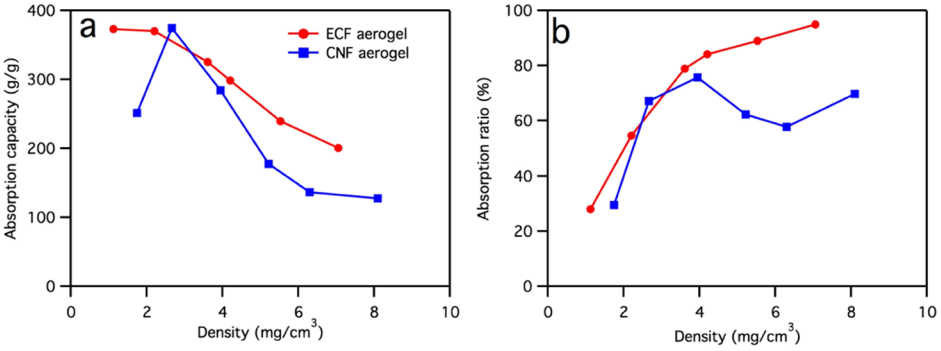

Figure 3. Comparison of liquid absorption performance between ECF and CNF aerogel with similar densities: (a) chloroform absorption capacity and (b) absorption ratio.

chloroform absorption that increased with decreasing aerogel densities (Figure 3a). The 373 g/g of absorption capacity (or 250 mL/g when normalized by chloroform density) is far higher than most of the aerogels reported to date, including those from natural polymers such as chitin (29−58 g/g),[49] ethyl cellulose (32−64 g/g),[50] gelatin (70−123 g/g),[51] bacterial cellulose (86−185 g/g),[52] microfibrillated cellulose (88−228 g/g),[36] and cellulose ester (112 g/g)[53] aerogels, synthetic polymers such as melamine (38−217 g/g),[54−56] poly(vinyl alcohol) (10−274 g/g),[35,57,58] and polystyrene (100−270 g/g),[59] carbonized natural polymers such as glucose nanofibers (40−115 g/g),[8] bacterial cellulose (106−312 g/g),[60] cotton (50−192 g/g),[61] poplar catkins (80−161 g/g),[62] waste paper (33−70 g/g),[63] and kapok fiber (147−292 g/g)[64]-based aerogels, and most of graphitic carbon such as carbon nanotubes (80−180 g/g)[65] and graphene (134−283 g/g)[66] (Table 1). Few aerogels with higher absorption capacity have been reported with graphene oxide/carbon nanotubes (215−913 g/g),[7] graphene framework (200−600 g/g),[67] and reduced graphene oxide/bacterial cellulose carbon aerogel (393−1002 g/g),[68] all containing energy-intensively produced graphene and carbon nanotubes, which inevitably increase the production cost of the absorbents. Other than these few graphene-based aerogels, the reported ECF aerogel demonstrates the highest absorption capacity among all polymeric and carbonized natural polymer-based aerogels. Carbonization of natural polymers (mostly cellulose) has also the drawback of losing significant material, that is, 49.4% of cellulose $(C_6H_{10}O_5)_n$ is O.

On the basis of the theoretical absorption capacity calculated from the density of aerogel, the actual chloroform absorption showed that over 95% of the pores within the 7 mg/cm^3 density aerogel was filled. This nearly complete accessibility of this ECF aerogel to chloroform is much higher than the 70% for CNF aerogel with a slightly higher density of 8.1 mg/cm^3 (Figure 3b). This significantly higher pore accessibility of the ECF aerogel by liquids was beneficial for the higher overall liquid absorption. The nearly full pore accessibility could be ascribed to the hierarchical pore structures of the ECF aerogels, with hundreds of micrometer wide large pores holding the absorbed liquid and the numerous tens of micrometer wide

DOI: 10.1021/acsomega.8b00144
ACS Omega 2018, 3, 3530−3539

Table 1. Comparison of Physical Properties and Absorption Capacity of Varied Superabsorbent Aerogel[a]

category	absorbent materials	density (mg/cm^3)	absorption capacity (g/g)	normalized maximum absorption capacity (mL/g)	refs
natural polymers	electrospun cellulose	1.1−7.0	201−373	250	this study
	chitin	21.2−24.3	29−58	39	49
	bacterial cellulose	6.69−6.77	86−185	124	52
	ethyl cellulose	18.9	32−64	43	50
	cellulose esters	4.3−110	112	140 normalized by kerosene oil	53
	gelatin	7.2	70−123	83	51
	microfibrillated cellulose	2.4−24.2	88−228	235 normalized by silicone oil	36
	cellulose nanofibrils	1.7−8.1	210−375	251	22
synthetic polymers	polyethylenimine	N/A	29−39	26	69
	carbonized lignin-coated melamine foam	6.4	98−217	146	54
	graphene-coated melamine foam	N/A	50−130	87	55
	PDVB-PDMS-coated melamine	N/A	38−123	82	56
	poly(vinyl alcohol)/carbon nanotube	27−83	10−52	35	57
	poly(vinyl alcohol)/graphene	3.3	130−274	184	58
	poly(vinyl alcohol)/cellulose nanofibrils	13.0	44−96	64	35
	polystyrene/carbon nanotubes	N/A	100−270	181	59
carbonized natural polymers	carbonized glucose nanofibers	3.3	40−115	72 normalized by phenoxin	8
	carbonized bacterial cellulose	4−6	106−312	208 normalized by phenoxin	60
	carbonized cotton	12	50−192	80	61
	carbonized poplar catkins	4.3	80−161	107	62
	carbonized waste paper	23.6	33−70	44 normalized by phenoxin	63
	carbonized kapok fibers	1	147−292	183 normalized by phenoxin	64
graphitic carbon	graphene aerogel	3.5	134−283	189	66
	carbon nanotubes	5−10	80−180	120	65
	graphene oxide/carbon nanotubes	0.16−7.6	215−913	570 normalized by phenoxin	7
	graphene framework	2.1	200−600	375 normalized by phenoxin	67
	reduced graphene oxide/bacterial cellulose carbon fiber	0.7−10.2	393−1002	626 normalized by phenoxin	68

[a]Note: unless specified, the normalized maximum absorption capacity was based on chloroform.

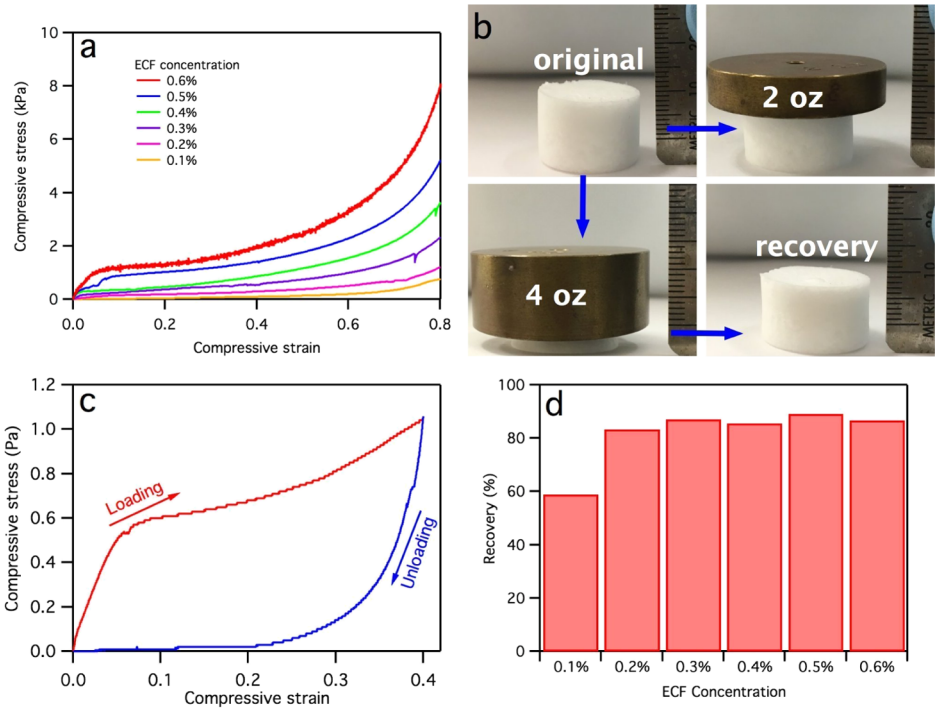

Figure 4. Mechanical performance of ECF aerogels: (a) compressive stress−strain curves; compression−recovery of aerogel with 4.2 mg/cm^3 density (from 0.4 wt % aq ECF dispersion): (b) digital images of under 2 (56.7 g) and 4 oz (113.4 g) weights; (c) compressive stress−strain hysteresis at 0.4 strain; and (d) recovery from compression under 4 oz weight.

DOI: 10.1021/acsomega.8b00144
ACS Omega 2018, 3, 3530−3539

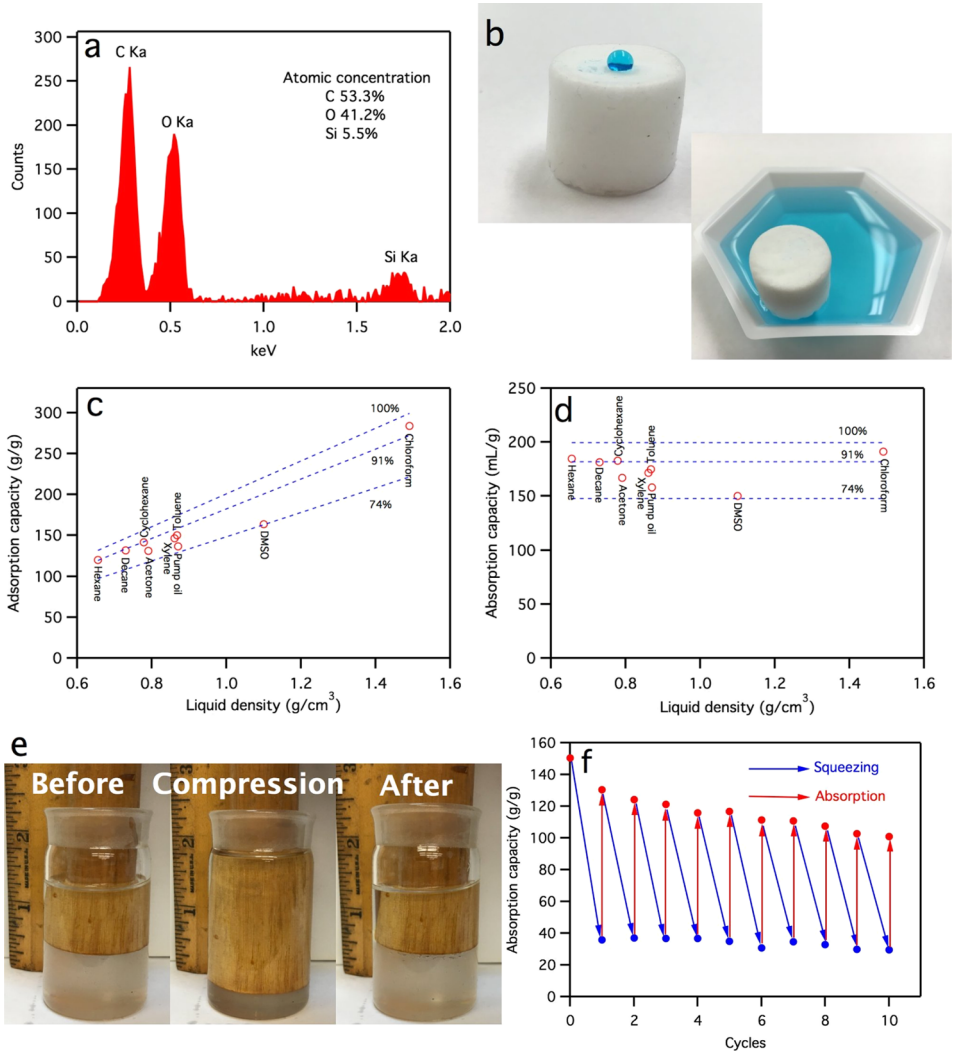

Figure 5. Characterization of silanized ECF aerogels (from 0.4 wt % aq ECF dispersion): (a) EDS spectra with atomic concentration for C, O, and Si; (b) digital images of water beads on aerogel and aerogel floating on the water surface (water was dyed with methylene blue to enhance visual contrast); (c) mass- (g/g) and (d) volume (mL/g)-based adsorption capacity toward varied organic liquids, with dash lines representing 74, 91, and 100% adsorption capacity calculated from (porosity × $\rho_{liquid}/\rho_{aerogel}$) in (c) and porosity/$\rho_{aerogel}$ in (d); (e) digital images showing aerogel in toluene before (left), during (middle), and after (right) compression; and (f) cyclic absorption of toluene during 10 cycles of absorption-squeezing.

small pores on the cell walls allowing liquid to be transported across the large pores. While the lack of interfiber association benefits organic liquid accessibility among the hierarchical pore structure in ECF aerogels, this and the lack of interfiber entanglement cause ready redispersion in water by gentle hand shaking into individual fibers (Figure S4, Supporting Information). Therefore, ECF aerogels could not retain the porous structures in water to be used for aqueous applications. This poor aqueous integrity of ECF aerogels is in distinct contrast to the wet resilient CNF aerogels, which could withstand over 100 compression−recovery cycles because of the strong interfibril association.[22]

In essence, the physical properties of these cellulose aerogels depend highly on the dimension of the nanofiber precursors as well as their crystalline structures, with the larger ECFs forming a open porous cellular structure with higher pore accessibilities but less aqueous stability, whereas the 3 orders of magnitude smaller CNFs self-assembled via strong interfibril association to achieve excellent aqueous stability, with the sacrifice of interpore accessibility.

All ECF aerogels remained intact when compressed at up to 0.8 strain in air (Figure 4a). These dry compressive stress−strain curves showed impressive ductile and flexible properties attributed to the large fiber sizes and the flexibility of ECF. Three distinct stages could be observed from the stress−strain curves, that is, the initial linear elastic regions at low strain (<0.05), followed by a nonlinear plastic deformation region once passing the yield stress, and the last densification stage at high strain. As expected, both the Young's modulus and ultimate stress increased with increasing aerogel densities, reaching 20.1 and 8.1 kPa, respectively, for the 0.6 ECF aerogel (Table S1, Supporting Information), respectively. While compressive stress−strain curves were similar in shape to cellulose nanofibrils aerogels,[18,22] these respective compression modulus and stress are less than half and one-third as compared to the CNF aerogels with similar density (54.5 and 25.3 kPa for Young's modulus and ultimate stress, respectively).[22] The significantly lower mechanical properties of the ECF aerogel can be attributed to the absence of interfiber association observed and discussed earlier as well as the weaker regenerated

DOI: 10.1021/acsomega.8b00144
ACS Omega 2018, 3, 3530−3539

cellulose II crystalline structure as compared to the native cellulose Iβ crystalline structure of the CNF aerogels.

Despite the lower compressive modulus and stress than the CNF aerogels, the ECF aerogel is sufficiently strong to withstand external forces, as demonstrated by a lack of appreciable deformation of a 25.2 mg aerogel under a 2 oz (56.7 g) weight, that is, 2250 times of its own mass (Figure 4b). Even under 4500 times of own mass or 4 oz (113.4 g) weight that significantly deforms ECF to ca. 70% in height, it still can recover to over 80% of its original shape upon releasing the load. The compression−recovery was further demonstrated by repetitively compressing the aerogel from the 0.4 wt % ECF concentration (density of 4.2 mg/cm^3), showing immediate recovery upon releasing the stress (Video S1, Supporting Information). The compressive stress−strain curves of the same aerogel at up to 0.4 strain showed gradual decrease in compressive stress upon releasing the load (Figure 4c), with a positive stress value at strain above 0.12, which demonstrates the recovery behavior of the aerogel upon releasing the compressive force. The large hysteresis between the loading and unloading curves indicates energy dissipation due to yielding. All ECF aerogels with densities above 2.2 mg/cm^3, that is, from ≥0.2 wt % ECF concentrations, could recover 83 to 89% when compressed by 113.4 g (4 oz) weight (Figure 4d). The relative lower 59% recovery for the aerogel from the 0.1 wt % concentration is due to its lower 1.1 mg/cm^3 density and weaker structure.

To retain aerogel integrity under an aqueous environment and enable selective oil removal from aqueous media, the aerogel was made hydrophobic by facile vapor deposition of methyltrichlorosilane, converting the hydrophilic surface hydroxyl groups to hydrophobic methyl groups. Successful silanization was confirmed from the presence of 5.5 at. % silicon by energy-dispersive spectrometry (EDS) spectra (Figure 5a), showing uniform coverage on fiber surfaces from Si mapping (Figure S5, Supporting Information). The acquired hydrophobicity was clearly shown by water beading up on the aerogel surface with a large contact angle as well as aerogel floating on the water surface without sinking or disintegration (Figure 5b). The silanized aerogel remained stable in water, in contrast to the complete disintegration of the untreated original.

The silanized ECF aerogel absorbed 119 to 284 g/g (or 171 to 191 mL/g) of nonpolar organic liquids, including aliphatic (hexane and decane), chlorinated (chloroform), cyclic (cyclohexane), and aromatic (toluene and xylene) hydrocarbons and oil (pump), corresponding to 86−96% of the theoretical absorption capacity (Figure 5c,d). These impressive absorption capacities are much higher than the 76% of the same nonpolar organic liquids absorbed by CNF aerogel,[22] again showing significantly improved pore accessibility. The absorption capacity is slightly lower for the polar dimethyl sulfoxide (DMSO) at 150 mL/g or 75% of the theoretical values but still higher than the 64% for CNF aerogels toward the same solvent.

Besides, the silanized ECF aerogel showed excellent flexibility and resilience in organic liquids, as demonstrated by full shape recovery when compressed and then released while immersed in toluene (Figure 5e). This superior wet resilience in organic liquids makes recovering of the oil absorbed easy, by simple squeezing and recycling, permitting reusing of the aerogel for absorbing the same or even a different liquid. It showed that a toluene-saturated aerogel could be squeezed to remove ∼80% of the absorbed (with ∼30 g/g remaining), then still retain over 67% of its original absorption capacity in 10 repetitive absorption-squeezing cycles (Figure 5f). Therefore, these ECF aerogels have shown to be excellent candidates for repetitive oil removal from aqueous media. The oil recovery by mechanical force is simple and less energy-intensive than distillation of the same from the CNF aerogel.[22]

To further demonstrate the ability of silane-modified ECF aerogel in oil−water separation, complete removal of oil contamination from water was shown by selectively absorbing either chloroform underneath the water by being forced under water without absorbing it along the way (Figure 6a, Video S2, Supporting Information) or toluene floating on the water surface (Figure 6b, Video S3, Supporting Information). In essence, the ECF aerogels exhibited super high liquid absorbency, showing nearly full pore accessibility, and excellent dry and wet resiliency, validating its application in oily contamination removal as well as recyclability.

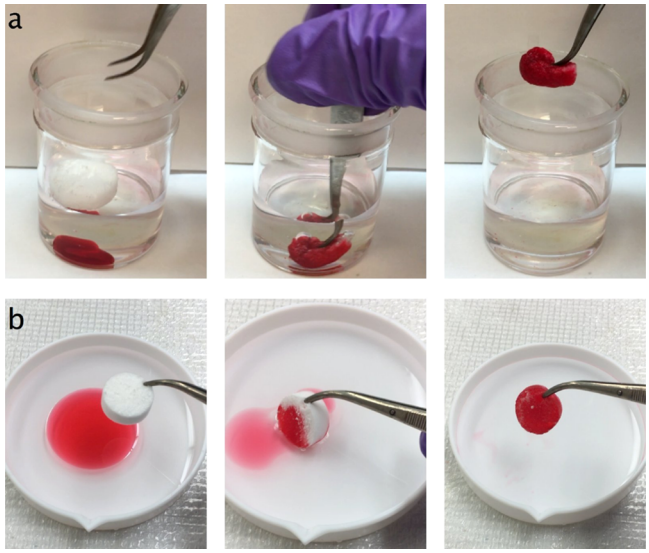

Figure 6. Demonstration of oil/water separation by silanized ECF aerogel (from 0.4 wt % aq ECF dispersion): sequential snapshot of removing (a) chloroform at the bottom and (b) toluene on the top of water; both liquids were dyed with Sudan IV to enhance the visibility.

Besides environmental remediation, the ECF aerogel also showed promising aspect in energy storage application, as demonstrated by using the carbonized ECF (C-ECF) aerogel as the electrode materials in a supercapacitor. C-ECF aerogel was obtained by heating the unmodified ECF aerogel at 10 °C/min to 800 °C and maintained at 800 °C for 30 min under a N_2 atmosphere. The C-ECF aerogel showed significant mass and volume reduction of 94.7 and 96.9%, respectively, but an intact structure. Carbonization turns the white cellulose aerogel into black carbon aerogel, with the atomic concentration of 97.1 and 2.9% for C and O, respectively. SEM images of the carbon aerogel also showed a 3D porous structure with pores of 20−100 μm, which is significantly lower than the several hundreds of microns sized pores in the original aerogels (Figure 7a,b. The fiber diameter also reduced from the original average 262 nm to around 100 nm width (Figure 7c). The carbon aerogel was tested for its performance in the supercapacitor by characterizing the binder and conductive additive-free C-ECF electrodes in 6 M KOH in symmetric coin cells. The cell voltage was set to be 1 V because of the limited electrochemical window of the aqueous electrolyte. Cyclic voltammogram was obtained and exhibited a rather rectangular shape, as shown in Figure 7d,

DOI: 10.1021/acsomega.8b00144
ACS Omega 2018, 3, 3530−3539

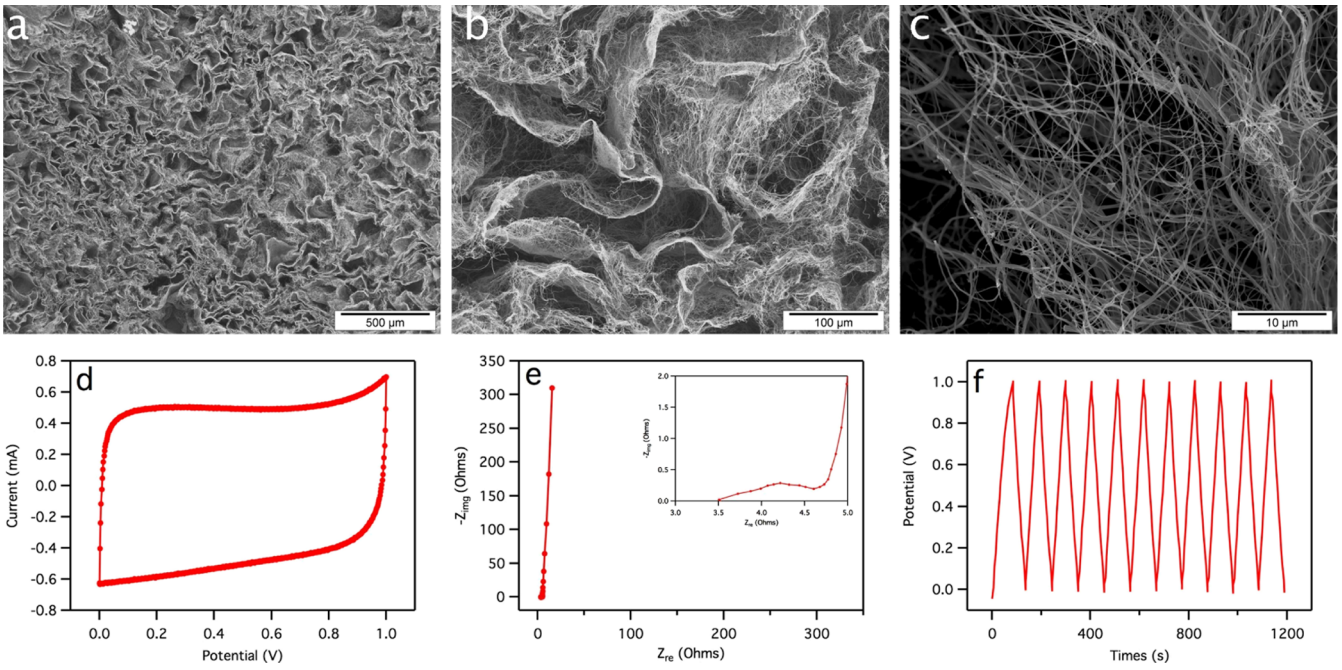

Figure 7. Morphological and electrochemical characterization of C-ECF aerogel: (a–c) SEM images, (d) cyclic voltammogram at 10 mV/s, (e) Nyquist plot under the frequency range of 0.01 Hz to 100 kHz, with an inset showing the high frequency region, and (f) constant current charge/discharge curves at 1 mA/cm^2.

which indicated a good capacitive energy storage behavior.[70] On the basis of the Nyquist plot at 1 kHz in Figure 7e, the equivalent series resistance (ESR) was determined to be 4.2 Ω, which is comparable to the ESR of 3.2[71] and 4.6 Ω[72] for graphene-based supercapacitors reported previously, implying good conductive behavior, less internal energy loss, and better power performance. According to the evaluation methods reported by Zhang and Pan,[70] the specific capacitance of the C-ECF electrode was calculated to be 103 F/g and 51.3 mF/cm^2 based on the constant current charge/discharge curves shown in Figure 7f. The specific capacitance of 103 F/g was significantly larger (>2×) than the previously reported specific capacitance of 35–F/g for unactivated carbon aerogel-based supercapacitors with KOH electrolytes[73−75] and comparable to that of carbon nanotube-based supercapacitors.[76−78] In addition, the triangular charge/discharge behavior supported the good capacitive energy storage behavior demonstrated in Figure 7f. Therefore, the 3D ECF aerogel demonstrates great promise for energy storage applications.

CONCLUSIONS

Ultralightweight (density as low as 1.1 mg/cm^3) and highly porous (up to 99.9% porosity) cellulose II aerogels were facilely fabricated by disintegrating ECFs by high-speed blending followed by freezing/freeze-drying in all aqueous-based homogenization and drying processes. The ECF aerogels demonstrated excellent dry resiliency, showing up to 89% shape recovery from high-strain compression (~70% strain). The ECF aerogel contains hierarchical porous structures of large hundreds of micrometer wide cellular porous networks surrounded by fibrous cell walls with small tens of micron wide pores, contributing to superior liquid absorption capacity and pore accessibility for liquid absorption, respectively. The ECF aerogels could absorb 201–373 g/g of chloroform, accounting for over 95% of the theoretical absorption capacity. Furthermore, the ECF aerogels could be facilely modified to be hydrophobic and stable in an aqueous environment by vapor phase silanization with methyltrichlorosilane and to be capable of selectively and repetitively removing nonpolar liquids (as demonstrated with chloroform and toluene) from aqueous media. The silanized ECF aerogel showed excellent shape recovery from compressing in toluene, maintaining over 67% of original absorption capacity after 10 repetitive absorption-squeezing cycles. This high absorption capacity and selectivity, as well as reusability, make these cellulose II aerogels excellent candidates for removing hydrocarbon/oily contamination from aqueous media and hydrocarbon/oil–water separation applications. A supercapacitor based on the CNF aerogel showed a very low ESR of 4.2 Ω and a high areal capacitance of 51.3 mF/cm^2. In essence, the ECF aerogel exhibited promising performance in both environmental remediation and energy storage, which could be further extended to more applications such as insulating materials, biomedical scaffolds, as well as electrochemical sensors.

EXPERIMENTAL SECTION

Materials. Cellulose acetate (M_n = 30 000 Da, 39.8 wt % acetyl content) was electrospun into fibrous membranes from 2:1 w/w acetone/DMAc at 15 wt % and then deacetylated in 0.05 M aqueous NaOH at ambient temperature for 24 h.[44] Methyltrichlorosilane (99%, Sigma-Aldrich), methylene blue (Certified biological stain, Fisher Scientific), hexane (Certified ACS, Fisher Scientific), decane (Certified, Fisher Scientific), cyclohexane (HPLC grade, EM Science), acetone (Histological grade, Fisher Scientific), xylene (GR ACS, EM Science), toluene (Certified ACS, Fisher Scientific), pump oil (Maxima C Plus, Fisher Scientific), DMSO (GR, EMD), and chloroform (Certified ACS, Fisher Scientific) were used as received without further purification. All water used was purified using a Milli-Q plus water purification system (Millipore Corporate, Billerica, MA).

DOI: 10.1021/acsomega.8b00144
ACS Omega 2018, 3, 3530–3539

Fabrication of ECF Aerogel. The electrospun cellulose membrane was cut into 5 × 5 mm pieces and then dispersed in water by high-speed blending (37 000 rpm, 5 min) into short fibers. ECF aerogel was fabricated from freezing (−20 °C, 5 h) 0.1−0.6 wt % aqueous dispersions of short ECF and then lyophilizing (−50 °C, 24 h) in a freeze-drier (FreeZone 1.0L Benchtop Freeze Dry System, Labconco, Kansas City, MO). The ECF aerogel made from 0.4 wt % cellulose fiber suspension was modified by vapor deposition of methyltrichlorosilane at 85 °C for 30 min in a vacuum oven.

Characterization of ECF Aerogel. The density (ρ_a) of ECF aerogel was calculated from its mass divided by the volume, and porosity of the aerogel was calculated as

$$\text{Porosity}\ (\%) = \left(1 - \frac{\rho_a}{\rho_c}\right) \times 100\% \quad (1)$$

where ρ_c is the density of cellulose taken as 1.6 g cm^{-3}.[45]

Liquid absorption capacity was determined by immersing the aerogel into each selected liquid until complete saturation. The absorption capacity (g/g) was calculated as

$$\text{Absorption capacity} = \frac{(w_s - w_0)}{w_0} \quad (2)$$

where w_s and w_0 are weights of fully saturated and dry aerogel, respectively.

The ECF aerogel was sputter-coated with gold and imaged by a field-emission scanning electron microscope (FESEM) (XL 30-SFEG, FEI/Philips, USA) at a 5 mm working distance and a 5 kV accelerating voltage. Elemental analysis of organosilane-modified ECF aerogel was conducted using EDS (EDAX, AMETEK, Inc.) attached on the FESEM. The samples were scanned at a 1000 magnification with a 5 kV accelerating voltage and a 5 mm working distance. The specific surface area and pore characteristics of ECF aerogel were determined by N_2 adsorption at 77 K by a surface area and porosity analyzer (ASAP 2000, Micromeritics, USA). The sample was degassed at 35 °C to below 16 mmHg. The specific surface was determined by the BET method from the linear region of the isotherms in the 0.06−0.20 relative P/P_0 pressure range. Pore size distributions were derived from the desorption branch of the isotherms by the Barrett−Joyner−Halenda method. XRD spectra for the ECF aerogel were collected on a Scintag XDS 2000 powder diffractometer using a Ni-filtered Cu Kα radiation (λ = 1.5406 Å) at an anode voltage of 45 kV and a current of 40 mA. Diffractograms were recorded from 5° to 40° at a scan rate of 2°/min.

The CrI was estimated using the Segal equation[46]

$$\text{CrI} = \frac{I_{020} - I_{am}}{I_{020}} \quad (3)$$

where I_{020} is the peak intensity of the 020 lattice plane located as 21.8° 2θ, and I_{am} is the intensity attributed to amorphous cellulose at 16° 2θ for cellulose II. Compressive tests were performed on 10 mm long cylindrical ECF aerogel using Instron 5566 equipped with a 2.5 N load cell and two flat-surface compression stages. The loading and unloading compressive rates were set to the same constant 1 mm/min.

Construction and Electrochemical Characterization of an ECF Aerogel-Based Supercapacitor. The ECF aerogel fabricated from 0.6 wt % cellulose nanofiber suspension was carbonized by heating at 10 °C/min to 800 °C and maintained at 800 °C for 30 min under a N_2 atmosphere, which was used for supercapacitor application. The C-ECF aerogel was used to prepare the supercapacitor electrode by applying ca. 1 mg of the material directly to 1 cm^2 nickel foam without a binder and conductive additive then roller-pressed to 50 μm thickness to improve the contact between C-ECF and nickel foam. Symmetric supercapacitor coin cells were constructed using two identical electrodes with cellulose filter paper as the separator and sealed with a manual crimper (CR2032, MTI). A 6 M KOH aqueous suspension was used as electrolytes.

The electrochemical properties of C-ECF supercapacitors were analyzed through cyclic voltammetry on a potentiostat/galvanostat (EG&G Princeton Applied Research, model 263A), galvanostatic charge/discharge on an eight channel battery analyzer (MTI Corporation, mode BST8-MA), and electrochemical impedance spectroscopy on a frequency response detector connected with the EG&G 263A with the frequency from 100 kHz to 10 mHz at room temperature.

■ ASSOCIATED CONTENT

Supporting Information

The Supporting Information is available free of charge on the ACS Publications website at DOI: 10.1021/acsomega.8b00144.

SEM images of ECF membranes and aerogels at different concentrations; BET specific surface area and pore size distribution of the ECF membrane; polarized light microscopy image of ECF aerogel being re-dispersed in water; mechanical properties of the ECF aerogels; and SEM and EDS Si mapping of silanized ECF aerogel (AVI)

Complete removal of oil contamination from water by selectively absorbing chloroform (AVI)

Complete removal of oil contamination from water by selectively absorbing toluene (AVI)

■ AUTHOR INFORMATION

Corresponding Author

*E-mail: ylhsieh@ucdavis.edu. Phone +1 530 752 0843. Fax: +1 530 752 7584 (Y.-L.H.).

ORCID

You-Lo Hsieh: 0000-0003-4795-260X

Present Address

†Department of Wood Science, The University of British Columbia, Vancouver, Canada V6T 1Z4 (F.J.).

Notes

The authors declare no competing financial interest.

■ ACKNOWLEDGMENTS

The authors appreciate the funding support from the AgTech Innovation Center at University of California, Davis.

■ REFERENCES

(1) Wen, D.; Liu, W.; Haubold, D.; Zhu, C.; Oschatz, M.; Holzschuh, M.; Wolf, A.; Simon, F.; Kaskel, S.; Eychmüller, A. Gold aerogels: Three-dimensional assembly of nanoparticles and their use as electrocatalytic interfaces. *ACS Nano* **2016**, *10*, 2559−2567.

(2) Zu, G.; Shen, J.; Zou, L.; Wang, W.; Lian, Y.; Zhang, Z.; Du, A. Nanoengineering super heat-resistant, strong alumina aerogels. *Chem. Mater.* **2013**, *25*, 4757−4764.

(3) Freytag, A.; Sánchez-Paradinas, S.; Naskar, S.; Wendt, N.; Colombo, M.; Pugliese, G.; Poppe, J.; Demirci, C.; Kretschmer, I.; Bahnemann, D. W.; Behrens, P.; Bigall, N. C. Versatile aerogel

DOI: 10.1021/acsomega.8b00144
ACS Omega 2018, 3, 3530−3539

fabrication by freezing and subsequent freeze-drying of colloidal nanoparticle solutions. *Angew. Chem., Int. Ed.* **2016**, *55*, 1200−1203.
(4) Si, Y.; Yu, J.; Tang, X.; Ge, J.; Ding, B. Ultralight nanofibre-assembled cellular aerogels with superelasticity and multifunctionality. *Nat. Commun.* **2014**, *5*, 5802.
(5) Wang, X.; Lu, L.-L.; Yu, Z.-L.; Xu, X.-W.; Zheng, Y.-R.; Yu, S.-H. Scalable template synthesis of resorcinol-formaldehyde/graphene oxide composite aerogels with tunable densities and mechanical properties. *Angew. Chem., Int. Ed.* **2015**, *54*, 2397−2401.
(6) Khan, Z. U.; Edberg, J.; Hamedi, M. M.; Gabrielsson, R.; Granberg, H.; Wågberg, L.; Engquist, I.; Berggren, M.; Crispin, X. Thermoelectric polymers and their elastic aerogels. *Adv. Mater.* **2016**, *28*, 4556−4562.
(7) Sun, H.; Xu, Z.; Gao, C. Multifunctional, ultra-flyweight, synergistically assembled carbon aerogels. *Adv. Mater.* **2013**, *25*, 2554−2560.
(8) Liang, H.-W.; Guan, Q.-F.; Chen, L.-F.; Zhu, Z.; Zhang, W.-J.; Yu, S.-H. Macroscopic-scale template synthesis of robust carbonaceous nanofiber hydrogels and aerogels and their applications. *Angew. Chem., Int. Ed.* **2012**, *51*, 5101−5105.
(9) Li, C.; Qiu, L.; Zhang, B.; Li, D.; Liu, C.-Y. Robust vacuum-/air-dried graphene aerogels and fast recoverable shape-memory hybrid foams. *Adv. Mater.* **2016**, *28*, 1510−1516.
(10) Kistler, S. S. Coherent expanded aerogels. *J. Phys. Chem.* **1932**, *36*, 52−64.
(11) Jin, H.; Nishiyama, Y.; Wada, M.; Kuga, S. Nanofibrillar cellulose aerogels. *Colloids Surf., A* **2004**, *240*, 63−67.
(12) Cai, J.; Zhang, L. Unique gelation behavior of cellulose in NaOH/Urea aqueous solution. *Biomacromolecules* **2006**, *7*, 183−189.
(13) Cai, J.; Kimura, S.; Wada, M.; Kuga, S.; Zhang, L. Cellulose aerogels from aqueous alkali hydroxide-urea solution. *ChemSusChem* **2008**, *1*, 149−154.
(14) Cai, J.; Liu, S.; Feng, J.; Kimura, S.; Wada, M.; Kuga, S.; Zhang, L. Cellulose-silica nanocomposite aerogels by in situ formation of silica in cellulose gel. *Angew. Chem., Int. Ed.* **2012**, *51*, 2076−2079.
(15) Yang, X.; Cranston, E. D. Chemically cross-linked cellulose nanocrystal aerogels with shape recovery and superabsorbent properties. *Chem. Mater.* **2014**, *26*, 6016−6025.
(16) De France, K. J.; Hoare, T.; Cranston, E. D. Reviews of hydrogels and aerogels containing nanocellulose. *Chem. Mater.* **2017**, *29*, 4609−4631.
(17) Yang, X.; Shi, K.; Zhitomirsky, I.; Cranston, E. D. Cellulose nanocrystal aerogels as universal 3D lightweight substrates for supercapacitor materials. *Adv. Mater.* **2015**, *27*, 6104−6109.
(18) Pääkkö, M.; Vapaavuori, J.; Silvennoinen, R.; Kosonen, H.; Ankerfors, M.; Lindström, T.; Berglund, L. A.; Ikkala, O. Long and entangled native cellulose I nanofibers allow flexible aerogels and hierarchically porous templates for functionalities. *Soft Matter* **2008**, *4*, 2492−2499.
(19) Jiang, F.; Hsieh, Y.-L. Super water absorbing and shape memory nanocellulose aerogels from TEMPO-oxidized cellulose nanofibrils via cyclic freezing-thawing. *J. Mater. Chem. A* **2014**, *2*, 350−359.
(20) Sakai, K.; Kobayashi, Y.; Saito, T.; Isogai, A. Partitioned airs at microscale and nanoscale: thermal diffusivity in ultrahigh porosity solids of nanocellulose. *Sci. Rep.* **2016**, *6*, 20434.
(21) Jiang, F.; Hsieh, Y.-L. Cellulose nanofibril aerogels: synergistic improvement of hydrophobicity, strength and thermal stability via cross-linking with diisocyanate. *ACS Appl. Mater. Interfaces* **2017**, *9*, 2825−2834.
(22) Jiang, F.; Hsieh, Y.-L. Amphiphilic superabsorbent cellulose nanofibril aerogels. *J. Mater. Chem. A* **2014**, *2*, 6337−6342.
(23) Cervin, N. T.; Aulin, C.; Larsson, P. T.; Wågberg, L. Ultra porous nanocellulose aerogels as separation medium for mixtures of oil/water liquids. *Cellulose* **2012**, *19*, 401−410.
(24) Hamedi, M.; Karabulut, E.; Marais, A.; Herland, A.; Nyström, G.; Wågberg, L. Nanocellulose aerogels functionalized by rapid layer-by-layer assembly for high charge storage and beyond. *Angew. Chem., Int. Ed.* **2013**, *52*, 12038−12042.
(25) Zhang, W.; Zhang, Y.; Lu, C.; Deng, Y. Aerogels from crosslinked cellulose nano/micro-fibrils and their fast shape recovery property in water. *J. Mater. Chem.* **2012**, *22*, 11642−11650.
(26) Zhang, Z.; Sèbe, G.; Rentsch, D.; Zimmermann, T.; Tingaut, P. Ultralightweight and flexible silylated nanocellulose sponges for the selective removal of oil from water. *Chem. Mater.* **2014**, *26*, 2659−2668.
(27) Korhonen, J. T.; Kettunen, M.; Ras, R. H. A.; Ikkala, O. Hydrophobic nanocellulose aerogels as floating, sustainable, reusable, and Recyclable Oil Absorbents. *ACS Appl. Mater. Interfaces* **2011**, *3*, 1813−1816.
(28) Chen, W.; Yu, H.; Li, Q.; Liu, Y.; Li, J. Ultralight and highly flexible aerogels with long cellulose I nanofibers. *Soft Matter* **2011**, *7*, 10360−10368.
(29) Nishino, T.; Takano, K.; Nakamae, K. Elastic-modulus of the crystalline regions of cellulose polymorphs. *J. Polym. Sci., Part B: Polym. Phys.* **1995**, *33*, 1647−1651.
(30) Eichhorn, S. J.; Young, R. J.; Davies, G. R. Modeling crystal and molecular deformation in regenerated cellulose fibers. *Biomacromolecules* **2005**, *6*, 507−513.
(31) Eichhorn, S. J.; Davies, G. R. Modelling the crystalline deformation of native and regenerated cellulose. *Cellulose* **2006**, *13*, 291−307.
(32) Kobayashi, Y.; Saito, T.; Isogai, A. Aerogels with 3D ordered nanofiber skeletons of liquid-crystalline nanocellulose derivatives as tough and transparent insulators. *Angew. Chem., Int. Ed.* **2014**, *53*, 10394−10397.
(33) Sehaqui, H.; Salajková, M.; Zhou, Q.; Berglund, L. A. Mechanical performance tailoring of tough ultra-high porosity foams prepared from cellulose I nanofiber suspensions. *Soft Matter* **2010**, *6*, 1824−1832.
(34) Erlandsson, J.; Duran, V. L.; Granberg, H.; Sandberg, M.; Larsson, P. A.; Wagberg, L. Macro- and mesoporous nanocellulose beads for use in energy storage devices. *Appl. Mater. Today* **2016**, *5*, 246−254.
(35) Zheng, Q.; Cai, Z.; Gong, S. Green synthesis of polyvinyl alcohol (PVA)-cellulose nanofibril (CNF) hybrid aerogels and their use as superabsorbents. *J. Mater. Chem. A* **2014**, *2*, 3110−3118.
(36) Wang, S.; Peng, X.; Zhong, L.; Tan, J.; Jing, S.; Cao, X.; Chen, W.; Liu, C.; Sun, R. An ultralight, elastic, cost-effective, and highly recyclable superabsorbent from microfibrillated cellulose fibers for oil spillage cleanup. *J. Mater. Chem. A* **2015**, *3*, 8772−8781.
(37) Yao, X.; Yu, W.; Xu, X.; Chen, F.; Fu, Q. Amphiphilic, ultralight, and multifunctional graphene/nanofibrillated cellulose aerogel achieved by cation-induced gelation and chemical reduction. *Nanoscale* **2015**, *7*, 3959−3964.
(38) Zhou, S.; Wang, M.; Chen, X.; Xu, F. Facile template synthesis of microfibrillated cellulose/polypyrrole/silver nanoparticles hybrid aerogels with electrical conductive and pressure responsive properties. *ACS Sustainable Chem. Eng.* **2015**, *3*, 3346−3354.
(39) Reneker, D. H.; Chun, I. Nanometre diameter fibres of polymer, produced by electrospinning. *Nanotechnology* **1996**, *7*, 216−223.
(40) Si, Y.; Fu, Q.; Wang, X.; Zhu, J.; Yu, J.; Sun, G.; Ding, B. Superelastic and superhydrophobic nanofiber-assembled cellular aerogels for effective separation of oil/water emulsions. *ACS Nano* **2015**, *9*, 3791−3799.
(41) Duan, G.; Jiang, S.; Jérôme, V.; Wendorff, J. H.; Fathi, A.; Uhm, J.; Altstädt, V.; Herling, M.; Breu, J.; Freitag, R.; Agarwal, S.; Greiner, A. Ultralight, soft polymer sponges by self-assembly of short electrospun fibers in colloidal dispersions. *Adv. Funct. Mater.* **2015**, *25*, 2850−2856.
(42) Huang, Y.; Lai, F.; Zhang, L.; Lu, H.; Miao, Y.-E.; Liu, T. Elastic carbon aerogels reconstructed from electrospun nanofibers and graphene as three-dimensional networked matrix for efficient energy storage/conversion. *Sci. Rep.* **2016**, *6*, 31541.
(43) Xu, T.; Miszuk, J. M.; Zhao, Y.; Sun, H.; Fong, H. Electrospun polycaprolactone 3D nanofibrous scaffold with interconnected and hierarchically structured pores for bone tissue engineering. *Adv. Healthcare Mater.* **2015**, *4*, 2238−2246.

DOI: 10.1021/acsomega.8b00144
ACS Omega 2018, 3, 3530−3539

(44) Liu, H.; Hsieh, Y.-L. Ultrafine fibrous cellulose membranes from electrospinning of cellulose acetate. *J. Polym. Sci., Part B: Polym. Phys.* **2002**, *40*, 2119−2129.
(45) Ganster, J.; Fink, H. P. In *Polymer Handbook*, 4th ed.; Brandrup, J., Immergut, E. H., Grulke, E. A., Eds.; Wiley & Sons: New York, 1999; pp V/135−V/157.
(46) Segal, L.; Creely, J. J.; Martin, A. E., Jr.; Conrad, C. M. An empirical method for estimating the degree of crystallinity of native cellulose using the x-ray diffractometer. *Text. Res. J.* **1959**, *29*, 786−794.
(47) Sèbe, G.; Ham-Pichavant, F.; Ibarboure, E.; Koffi, A. L. C.; Tingaut, P. Supramolecular structure characterization of cellulose II nanowhiskers produced by acid hydrolysis of cellulose I substrates. *Biomacromolecules* **2012**, *13*, 570−578.
(48) Isogai, A.; Usuda, M.; Kato, T.; Uryu, T.; Atalla, R. H. Solid-state CP MAS C-13 NMR-study of cellulose polymorphs. *Macromolecules* **1989**, *22*, 3168−3172.
(49) Duan, B.; Gao, H.; He, M.; Zhang, L. Hydrophobic modification on surface of chitin sponges for highly effective separation of oil. *ACS Appl. Mater. Interfaces* **2014**, *6*, 19933−19942.
(50) Lu, Y.; Yuan, W. Superhydrophobic/superoleophilic and reinforced ethyl cellulose sponges for oil/water separation: synergistic strategies of crosslinking, carbon nanotube composite, and nanosilica modification. *ACS Appl. Mater. Interfaces* **2017**, *9*, 29167−29176.
(51) Wang, J.; Zhao, D.; Shang, K.; Wang, Y.-T.; Ye, D.-D.; Kang, A.-H.; Liao, W.; Wang, Y.-Z. Ultrasoft gelatin aerogels for oil contaminant removal. *J. Mater. Chem. A* **2016**, *4*, 9381−9389.
(52) Sai, H.; Fu, R.; Xing, L.; Xiang, J.; Li, Z.; Li, F.; Zhang, T. Surface modification of bacterial cellulose aerogels' web-like skeleton for oil/water separation. *ACS Appl. Mater. Interfaces* **2015**, *7*, 7373−7381.
(53) Tripathi, A.; Parsons, G. N.; Rojas, O. J.; Khan, S. A. Featherlight, mechanically robust cellulose ester aerogels for environmental remediation. *ACS Omega* **2017**, *2*, 4297−4305.
(54) Yang, Y.; Yi, H.; Wang, C. Oil absorbents based on melamine/lignin by a dip adsorbing method. *ACS Sustainable Chem. Eng.* **2015**, *3*, 3012−3018.
(55) Ji, C.; Zhang, K.; Li, L.; Chen, X.; Hu, J.; Yan, D.; Xiao, G.; He, X. High performance graphene-based foam fabricated by a facile approach for oil absorption. *J. Mater. Chem. A* **2017**, *5*, 11263−11270.
(56) Li, Y.; Zhang, Z.; Wang, M.; Men, X.; Xue, Q. One-pot fabrication of nanoporous polymer decorated materials: from oil-collecting devices to high-efficiency emulsion separation. *J. Mater. Chem. A* **2017**, *5*, 5077−5087.
(57) Ma, C.-B.; Du, B.; Wang, E. Self-crosslink method for a straightforward synthesis of poly(vinyl alcohol)-based aerogel assisted by carbon nanotube. *Adv. Funct. Mater.* **2017**, *27*, 1604423.
(58) Ye, S.; Liu, Y.; Feng, J. Low-density, mechanical compressible, water-induced self-recoverable graphene aerogels for water treatment. *ACS Appl. Mater. Interfaces* **2017**, *9*, 22456−22464.
(59) Gu, J.; Xiao, P.; Chen, J.; Liu, F.; Huang, Y.; Li, G.; Zhang, J.; Chen, T. Robust preparation of superhydrophobic polymer/carbon nanotube hybrid membranes for highly effective removal of oils and separation of water-in-oil emulsions. *J. Mater. Chem. A* **2014**, *2*, 15268−15272.
(60) Wu, Z.-Y.; Li, C.; Liang, H.-W.; Chen, J.-F.; Yu, S.-H. Ultralight, flexible, and fire-resistant carbon nanofiber aerogels from bacterial cellulose. *Angew. Chem., Int. Ed.* **2013**, *52*, 2925−2929.
(61) Bi, H.; Yin, Z.; Cao, X.; Xie, X.; Tan, C.; Huang, X.; Chen, B.; Chen, F.; Yang, Q.; Bu, X.; Lu, X.; Sun, L.; Zhang, H. Carbon fiber aerogel made from raw cotton: A novel, efficient and recyclable sorbent for oils and organic solvents. *Adv. Mater.* **2013**, *25*, 5916−5921.
(62) Li, L.; Hu, T.; Sun, H.; Zhang, J.; Wang, A. Pressure-sensitive and conductive carbon aerogels from poplars catkins for selective oil absorption and oil/water separation. *ACS Appl. Mater. Interfaces* **2017**, *9*, 18001−18007.
(63) Li, L.; Li, B.; Sun, H.; Zhang, J. Compressible and conductive carbon aerogels from waste paper with exceptional performance for oil/water separation. *J. Mater. Chem. A* **2017**, *5*, 14858−14864.
(64) Zhang, J.; Li, B.; Li, L.; Wang, A. Ultralight, compressible and multifunctional carbon aerogels based on natural tubular cellulose. *J. Mater. Chem. A* **2016**, *4*, 2069−2074.
(65) Gui, X.; Wei, J.; Wang, K.; Cao, A.; Zhu, H.; Jia, Y.; Shu, Q.; Wu, D. Carbon nanotube sponges. *Adv. Mater.* **2010**, *22*, 617−621.
(66) Li, L.; Li, B.; Zhang, J. Dopamine-mediated fabrication of ultralight graphene aerogels with low volume shrinkage. *J. Mater. Chem. A* **2016**, *4*, 512−518.
(67) Zhao, Y.; Hu, C.; Hu, Y.; Cheng, H.; Shi, G.; Qu, L. A versatile, ultralight, nitrogen-doped graphene framework. *Angew. Chem., Int. Ed.* **2012**, *51*, 11371−11375.
(68) Li, C.; Wu, Z.-Y.; Liang, H.-W.; Chen, J.-F.; Yu, S.-H. Ultralight multifunctional carbon-based aerogels by combining graphene oxide and bacterial cellulose. *Small* **2017**, *13*, 1700453.
(69) Chatterjee, S.; Gupta, S. S.; Kumaraswamy, G. Omniphilic polymeric sponges by ice templating. *Chem. Mater.* **2016**, *28*, 1823−1831.
(70) Zhang, S.; Pan, N. Supercapacitors performance evaluation. *Adv. Energy Mater.* **2015**, *5*, 1401401.
(71) Wang, Y.; Shi, Z.; Huang, Y.; Ma, Y.; Wang, C.; Chen, M.; Chen, Y. Supercapacitor devices based on graphene materials. *J. Phys. Chem. C* **2009**, *113*, 13103−13107.
(72) Zhu, Y.; Murali, S.; Stoller, M. D.; Ganesh, K. J.; Cai, W. W.; Ferreira, P. J.; Pirkle, A.; Wallace, R. M.; Cychosz, K. A.; Thommes, M.; Su, D.; Stach, E. A.; Ruoff, R. S. Carbon-based supercapacitors produced by activation of graphene. *Science* **2011**, *332*, 1537−1541.
(73) Mayer, S. T.; Pekala, R. W.; Kaschmitter, J. L. The aerocapacitor: an electrochemical double-layer energy-storage device. *J. Electrochem. Soc.* **1993**, *140*, 446−451.
(74) Pekala, R. W.; Farmer, J. C.; Alviso, C. T.; Tran, T. D.; Mayer, S. T.; Miller, J. M.; Dunn, B. Carbon aerogels for electrochemical applications. *J. Non-Cryst. Solids* **1998**, *225*, 74−80.
(75) Kim, S. J.; Hwang, S. W.; Hyun, S. H. Preparation of carbon aerogel electrodes for supercapacitor and their electrochemical characteristics. *J. Mater. Sci.* **2005**, *40*, 725−731.
(76) Niu, C.; Sichel, E. K.; Hoch, R.; Moy, D.; Tennent, H. High power electrochemical capacitors based on carbon nanotube electrodes. *Appl. Phys. Lett.* **1997**, *70*, 1480−1482.
(77) Du, C.; Pan, N. Supercapacitors using carbon nanotubes films by electrophoretic deposition. *J. Power Sources* **2006**, *160*, 1487−1494.
(78) Du, C.; Yeh, J.; Pan, N. High power density supercapacitors using locally aligned carbon nanotube electrodes. *Nanotechnology* **2005**, *16*, 350−353.

DOI: 10.1021/acsomega.8b00144
ACS Omega 2018, 3, 3530−3539